Alena MIKITCHUK, Konstantin KOZADAEV

Belarusian State University, Belarus

doi:10.15199/48.2020.03.29

Comprehensive theoretical study of optical, thermophysical and acoustic properties of surface nanostructures with metallic nanoparticles for fiber-optic photoacoustic ultrasound transducers

Abstract. *The relationship between microscopic parameters of surface nanostructure and output characteristics of the photoacoustic transducer is established in this paper. In this paper, novel results in the area of complex simulation of thermal, acoustic and mechanical characteristics of surface nanostructures are demonstrated. The design of fiber-optic photoacoustic ultrasound transducer providing the most effective optical-to-acoustic conversion (intensity modulated optical signal is converted into pressure waves) is proposed as a result comprehensive theoretical study of absorbed optical power, stationary and non-stationary temperature and pressure distribution in various surroundings for different sets of microscopic parameters of surface nanostructures on the optical fiber edge. Additionally, the photoacoustic response is measured in order to provide the experimental proof of main results. Obtained dependencies can be used in the design of modern and perspective systems of ultrasound technical diagnostics, high-resolution ultrasound imaging of industrial densely-packed objects.*

Streszczenie. *W pracy przedstawiono zależność między parametrami mikroskopowymi nanostruktury powierzchniowej a wyjściowymi właściwościami akustycznymi przetwornika fotoakustycznego. W tym artykule przedstawiono nowatorskie wyniki w dziedzinie złożonej symulacji termicznych, akustycznych i mechanicznych właściwości nanostruktur powierzchniowych. Proponuje się zaprojektowanie światłowodowego fotoakustycznego przetwornika ultradźwiękowego zapewniającego najskuteczniejszą konwersję optyczno-akustyczną (sygnał optyczny o modulowanym natężeniu zamienia się w fale ciśnieniowe) w wyniku kompleksowych badań teoretycznych pochłoniętej mocy optycznej, stacjonarnej i niestacjonarnej temperatury oraz rozkład ciśnienia w różnych środowiskach dla różnych zestawów parametrów mikroskopowych powierzchniowych nanostruktur na krawędzi światłowodu. Dodatkowo mierzona jest odpowiedź fotoakustyczna w celu dostarczenia eksperymentalnego dowodu głównych wyników. Uzyskane zależności można wykorzystać przy projektowaniu nowoczesnych i perspektywicznych systemów ultradźwiękowej diagnostyki technicznej, obrazowania ultradźwiękowego wysokiej rozdzielczości gęsto upakowanych obiektów przemysłowych.* ***Analiza właściwościi optycznych, termicznych i akustycznych nanostruktury przeznaczonej do konstrukcji czujnika światłowodowego***

Keywords: Photoacoustic generation, metal nanoparticles, surface plasmon resonance, electromagnetic simulation, thermal simulation,
Słowa kluczowe: Generowanie fotoakustyczne, monowarstwa nanocząstek metali, rezonans powierzchniowy plazmonowy,.

Introduction

There are a number of methods of non-destructive testing [1-6] suitable for breakdown diagnostics of technical equipment, industrial machines and mechanisms [6], as well as eliminate defects in products manufactured [5-6]. One of the main approaches is the use of ultrasound signals as a diagnostic tool [6-8]. Compared with other methods of non-destructive testing, this method has a set of important advantages: high sensitivity (it is especially sensitive to the most dangerous type of cracks defects); low cost; safety for humans (unlike x-ray inspection); possibility of non-destructive testing without interruption of technological process; possibility to control wide range of materials [8]. It should be noted that methods of ultrasound diagnostics are often used when it is necessary to obtain high-resolution images (access to microwave assemblies, quality control of small microwave products and control of surface of high-Q cavities [8,9], medical and biological testing [10]). However, in many cases, the access to micro-soldered parts, and interconnects in integrated circuits is need, but it is very complicated due to conventional massive non-destructive testing ultrasound setups.

Conventional piezoelectric electro-acoustic transducers are characterized by high supply voltages, large size and high weight, high electromagnetic interference susceptibility, relatively narrow operation bandwidth [7, 11-13]. Photoacoustic transducers are very attractive alternative to electro-acoustic transducers. In photoacoustic transducers, absorber is heated and cooled, leading to mechanical deformations, which cause cycles of pressure, or, in the other words, acoustic waves in ambient surrounding [14,15]. However, the performance of such photoacoustic transducers is significantly limited by following factors. The bandwidth of the acoustic signal depends on the thickness of the absorber. Moreover, the small size of the photoacoustic transducer is one of the key factors in the applicability of the ultrasound source [16, 17]. In order to minimize the thickness of the absorbing layer in ultrasound transducers, surface nanostructures based on monolayers of noble metal nanoparticles (NPs) can be used [14 – 18].

Photoacoustic fiber-optic transducers are named between promising design directions for modern ultrasound generators [16-21]. The possibility of creating as well as some practical applications of photoacoustic fiber-optic transducers, based on NPs monolayers, have already been demonstrated [20-26]. However, the physical aspects and processes accompanying the absorbtion of modulated optical signal as well as heat transfer within the surface nanostructure have not been studied enough recently [27]. Additionally, test structure synthesis during the search of the optimal photoacoustic transducer design is rather expensive and long [27-29]. To achieve the highest absorbtion, it is important that the laser emission frequency be as close as possible to the spectral position of the maximum in the nanostructure absorbtion spectrum. Typically, the noble NPs monolayer deposited on the optical fiber edge has intense maxima in the absorbtion spectrum associated with the localized surface plasmon resonance phenomenon [30]. Note, that in the literature the term “localized” is often omitted and the abbreviated term “surface plasmon resonance” (SPR) is used [30], additionally, in the paper, the term “surface nanostructure” is used for noble NPs monolayer deposited on the optical fiber edge.

From the viewpoint of maximal value of absorbed optical modulated power, the most effective conversion is possible under a set of necessary conditions: the availability of high-frequency modulated lasers in the desired wavelength range (near the wavelength of the SPR absorbtion peak); a

wide SPR peak in the optical absorbtion spectrum (allows the usage of wavelength division multiplexing); high absorbtion coefficient at the SPR peak in the nanostructure spectrum [31–33]. In this case, the fraction of absorbed intensity modulated optical signal is the initial data for solving thermophysical (calculation of heat transient times) and, in turn, mechanical problems (temporal pressure distributions). The relationship between microscopic parameters of surface nanostructure and output parameters of photoacoustic transducer based on them is not explicit function, therefore, comprehensive theoretical study of optical, thermophysical and acoustic properties of such nanostructures with metallic NPs is need to be performed.

The purpose of the paper is to find out the relationship between microscopic parameters of surface nanostructure and output characteristics of the photoacoustic transducer. In this paper, the design of fiber-optic photoacoustic ultrasound transducer providing the most effective optical-to-acoustic conversion (intensity modulated optical signal is converted into pressure waves) is proposed as a result comprehensive theoretical study of absorbed optical power, stationary and non-stationary temperature and pressure distribution in various surroundings for different sets of microscopic parameters of surface nanostructures on the optical fiber edge. Additionally, the photoacoustic response is measured in order to provide the experimental proof of main results of the paper.

Obtained results can be used in the design of modern and perspective systems of ultrasound technical diagnostics, high-resolution ultrasound imaging of industrial densely-packed objects.

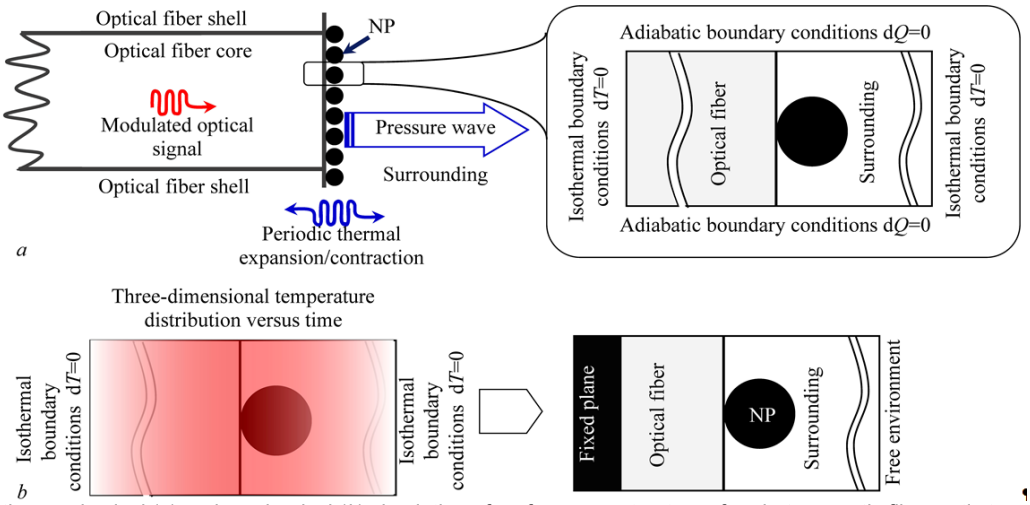

Fig.1. Layout of thermophysical (*a*) and mechanical (*b*) simulation of surface nanostructures for photoacoustic fiber-optic transducers

Comprehensive approach for theoretical study of surface nanostructures

In the case of fiber-optic photoacoustic transducer, laser driver provides generation of intensity-modulated optical signal, which is absorbed at optical fiber edge. Absorber (monolayer of NPs) is heated and cooled, leading to the local pressure modulation, which, in turn, results in generation of ultrasound acoustic waves. At least, the following simulation sequence should be performed in order to find out the relationship between the modulated optical power and the output acoustic characteristics of the photoacoustic transducer:

1. Calculate the optical absorbtion coefficient in the surface nanostructure at the optical fiber edge for an emission wavelength of commercially available laser (electromagnetic simulation has been studied in details by authors in the [31,34]);
2. Calculate available heat emission power for the some laser type and for each set of nanostructure microscopic parameters (available heat emission power is equal to the product of absorbtion coefficient and laser power [34]);
3. Simulate steady-state temperature distribution within the nanostructure for stationary value of heat emission power in order to check the possibility of physical implementation of such structures with long-term operation without overheating (steady-state thermal modelling);
4. For time-varying heat emission power, simulate a time-varying temperature distribution in the nanostructure and its surrounding. During this stage, durations of heat transfer transients are determined by means of analysis of the set of instantaneous temperature and heat flux 3D distributions;
5. Simulate mechanical displacements of the nanostructure components and resulting time-varying pressure (mechanical modeling).

Thermophysical simulation of photoacoustic transducers (2-4) is a multi-step process. Firstly, it is necessary to define the limitations numerical model of the nanostructure. Then, set the boundary conditions should be chosen. Photoacoustic transducer consisting of monolayer of monodisperse metal NPs on a substrate (optical fiber edge) has been simulated with the CST Microwave Studio SE [31, 35]. Surface nanostructure simulation is realized using the unit cell boundary conditions (translation is carried out in two dimensions to infinity). The unit cell of the nanostructure consists of four contiguous parallelepipeds, two of which consist of a substrate material, and the other two contain a surrounding material. NPs are placed at the interface between substrate and surrounding (with the base touching the substrate). The usage of additional parallelepipeds of the same material is associated with better convergence and limited processing power [35], remaining two layers are semi-infinite due to absorbing boundary conditions [39–42]. Nevertheless, random spatial distribution of NPs on the solid substrate results in slightly wider SPR-peak with decreased intensity. It is noted [38], that the main spectral parameters (e.g., SPR-peak position, absorbtion coefficient at the SPR-peak and its width) are changed no more then on the amount of 10–20% [38].

After, it is necessary to calculate steady-state as well as time-varying temperature distribution in the nanostructure and its surrounding. Figure 1*a* shows layout of thermophysical simulation of surface nanostructures for photoacoustic fiber-optic transducers. As it was shown

previously, surface nanostructure is characterized by very high aspect ratio [31]. Therefore, uniform temperature distribution boundaries can be used at some distance from the monolayer of NPs. In the case of heat transfer problems, such approximation can be used in planes, which are parallel to optical fiber edge and are situated at the distance exceeding 5-10 NP diameters. This allow to use isothermal boundary conditions, which is physically equivalent to the presence of an infinite heat reservoir.

Actually, the volume of the nanostructure at the optical fiber edge is negligible (for example, at least, several tens of centimeters of optical fiber correspond to the relative volume fraction of the nanostructure 10^{-12} - 10^{-13}). Previously, the authors found that an ordered electromagnetic field distribution is formed near the mode spot center at the optical fiber edge [31, 40–42, 46]. For this reason, it can be assumed that there is no heat transfer along the plane, which is parallel to the optical fiber edge. At least, there is no significant heat transfer between the NPs. Therefore, it is possible to apply adiabatic boundary conditions in use in the plane between NPs, which is orthogonal to optical fiber edge.

Figure 1*b* shows layout of mechanical simulation of surface nanostructures for photoacoustic fiber-optic transducers. Mechanical parameters of the media (Young's modulus, Poisson's ratio, coefficient of thermal expansion) are set and, a plane parallel to the optical fiber edge is fixed for implementation a mechanical model of a nanostructure as part of a photoacoustic transducer After, the 3D time-varying temperature distribution is taken into account. As a result of mechanical modeling, the strain tensor is calculated, as well as the tensor of mechanical stresses. Pressure is the hydrostatic stress, which is the average of the diagonal elements of the tensor of mechanical stresses.

Optical characteristics of surface nanostructures

The performance of the optical power absorbtion by surface nanostructure is determined by the set of factors. 1. commercially available lasers are required to generate modulated optical signal at the SPR-peak. 2. SPR-peak width at the level of 0.9 should exceed at least 25 nm [31] in order to use wavelength division multiplexing. 3. High value of the absorbtion coefficient at the SPR-peak is required. It should be noted that the absorbtion spectrum has been simulated for the wavelength range of 300–900 nm, where SPR-peaks are located typically [30, 43]. Within named wavelength range, photoacoustic transducers can be designed for either solid state lasers with frequency conversion (wavelength of 532 nm), or direct generation semiconductor lasers (wavelengths in the range 510 – 530 nm, 405 nm, 445 nm, 450 nm).

Figure 2 shows sets of nanostructure microscopic parameters, which provide the maximal value of absorbed optical modulated power. Further in paper, 2D-dependences of electromagnetic or thermophysical parameters on the microscopic parameters of the nanostructure are drown as level lines. Note that Ag and Au NPs are chosen because they are characterized by the most intense maxima in the optical absorbtion spectrum and are less susceptible to environmental influences [17, 41]. One can see that the highest value of absorbed optical power for nanostructures with Au NPs at the optical fiber edge in water is observed for NPs radius in the range of 18 – 23 nm and any value of the surface occupation density in the range of 35 – 70%.

The highest value of absorbed optical modulated power for nanostructures with Au NPs at the optical fiber edge in air is observed for NPs radius in the range of 12 – 22 nm and surface occupation density in the range of 53 – 70%. Additionally, there are some smaller sets of nanostructure parameters, which provide the maximal value of absorbed optical power for Au NPs in air.

Available heat emission power is equal to the product of absorbtion coefficient allows one to obtain initial data for solving thermophysical problem.

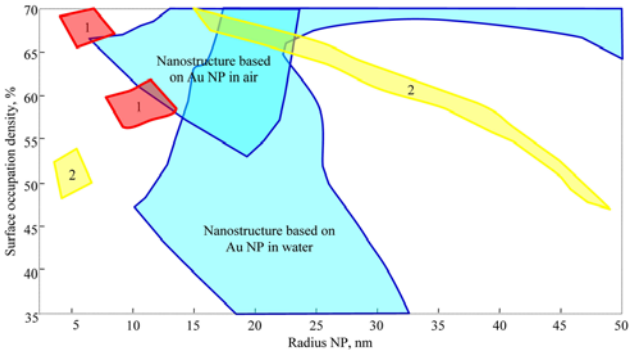

Fig.2. Sets of nanostructure microscopic parameters, which provide the maximal value of absorbed optical modulated power, where 1 is parameter region for nanostructures with NP Ag within air, 2 is for the same nanostructure within water

To estimate the available heat emission power, we used simulation data for Au and Ag NPs monolayers at optical fiber edge in water surrounding. To describe the laser, the following typical parameters of direct generation laser diodes are used: wavelengths of 520 nm and 445 nm and powers P_{opt} of 120 mW and 1800 mW, respectively. It should be noted that named peak optical powers have been used to calculate the theoretical maximum absorbed power or, in the other words, available heat emission power.

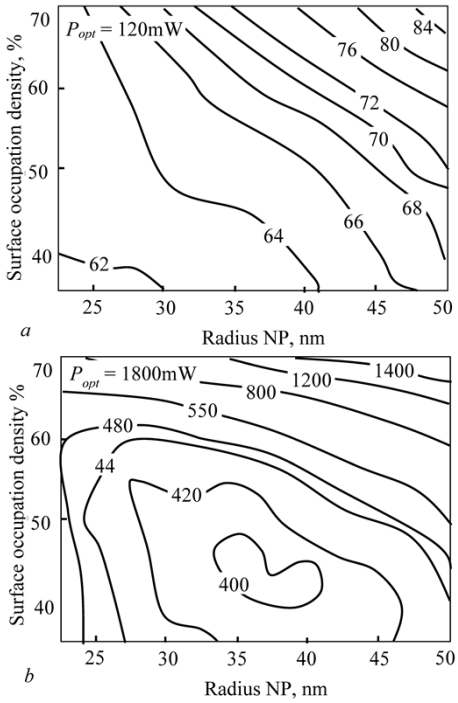

Fig.3. Heat emission power P_{opt} versus radius and surface occupation density of the spherical Au (*a*) and Ag (*b*) NPs at the optical fiber edge within water, when the laser emission wavelength is 520 nm (*a*) and 445 nm (*b*)

Figure 3 shows heat emission power versus radius and surface occupation density of the spherical Au and Ag NPs at the optical fiber edge within water, when the laser

emission wavelength is 520 nm and 445 nm. One can see that heat emission power of 80 mW (more than 60% of the laser power) and 1400 mW (over 70% of the laser power) can be achieved in the case of a nanostructures with Au and Ag NPs respectively. In the case of nanostructures with Ag NPs, there are some rather small sets of nanostructure microscopic parameters, which provide the maximal value of absorbed optical modulated power. For example, NP radii from 8 to 15 nm and surface occupation density from 57 to 62% provides the maximal value of absorbed optical modulated power for nanostructure in air surrounding.

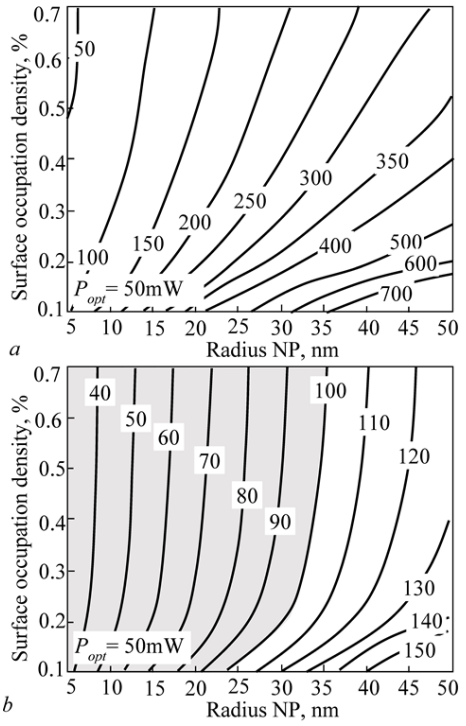

Fig.4. Value of temperature spatial maximum [°C] versus radius and surface occupation density of the spherical Au NPs at the optical fiber edge within air (*a*) and water (*b*) [heat emission power P_{opt} = 50mW]

Thermophysical characteristics

Simulation of the 3D time-varying temperature distributions for surface nanostructures with spherical metal NPs allows calculate temperature transients at different spatial points in the nanostructure. Additionally, transient time of the spatial temperature maximum can be calculated. Due to high aspect ratio of surface nanostructures under consideration, heat emission power is assumed to be released within NPs. In order to study the thermophysical characteristics, it was considered that either steady heat emission power is 50 mW or pulsed heat emission power is released in a nanostructure with the paek value of 50 mW, duration of 500 ns and pulse duty cycle of 2.

At least, maximal operation temperature in nanostructures with metal NPs should be limited by the melting points of metals or boiling point of the surrounding, whichever is the lower for water. In the steady state case for air, maximal operation temperature should be limited to the melting points of silver and gold, which are 961.9°C and 1064.4°C respectively. In the case of nanostructure in water, named temperature should be limited to the boiling point of water in order to avoid phase boundaries.

Figure 4 shows value of temperature spatial maximum versus radius and surface occupation density of the spherical of the spherical Au NPs at the optical fiber edge within air and water. The maximum temperature for simulated nanostructures in air increases with increasing of NP radius at the constant surface occupation density. In particular, the maximum temperature decreases from 250°C to 100°C for surface nanostructures with Au NPs radius of 15 nm; the maximum temperature decreases from 700°C to 260°C for surface nanostructures with Au NPs radius of 40 nm – both with change of surface occupation density in range of 10 – 70%.

One can see that nanostructure local temperature maximum value does not exceed 700°C for air surrounding. As a result, even theoretically, the applicability of such nanostructures is not limited by overheating. The maximum temperature for simulated nanostructures in air decreases with increasing of surface occupation density at the constant NP radius.

Microscopic parameters set, in which phase transient in water (boiling) do not occur for nanostructures with Au NPs in water, are described by the following parameters: NP radii from 5 to 25 nm and surface occupation density from 10 to 20%; NP radii from 5 to 30 nm and surface occupation density from 20 to 40%, as well as radii from 5 to 35 nm and surface occupation density from 40 to 70% (Figure 4*b*). For nanostructures in water, increase of the surface occupation density with a constant NP radius results in the decreasing of the maximum temperature. However, increase of NP radius with a constant surface occupation density results in the increasing of the maximum temperature. The maximum temperature decreases from 70°C to 54°C for surface nanostructures with NPs radius of 15 nm; the maximum temperature decreases from 100°C to 78°C for surface nanostructures with NPs radius of 25 nm – both with change of surface occupation density in range of 10 – 70%.

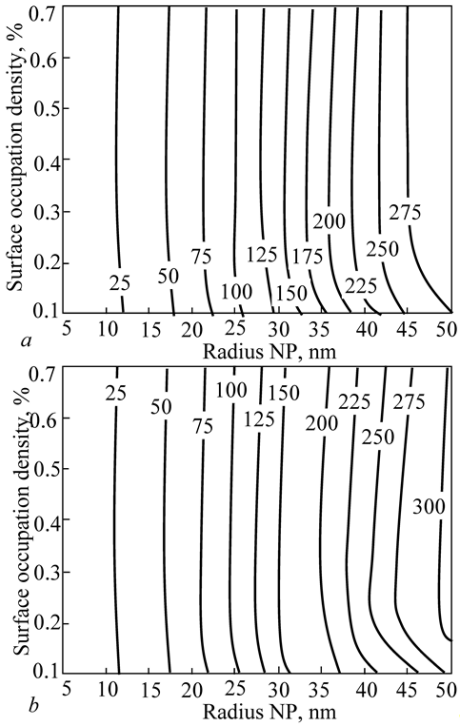

Fig.5. Rise (*a*) and fall (*b*) time for temperature spatial maximum versus radius and surface occupation density of the spherical Ag NPs at the optical fiber edge within water

Thus, the temperature of the surface nanostructure in fiber-optic photoacoustic transducer, when heat emission power is 50 mW, is most affected by the NP size, at the same time, surface occupation density is less important factor. Under studied conditions, the applicability of

nanostructures as photoacoustic transducer is not limited in air by thermal destruction of the nanostructure, while for nanostructures in water the thermophysical limitations are explained by boiling. In particular, for nanostructures based on NPs with radius exceeding 22 – 32 nm (depending on the surface occupation density) in water there is overheating which is explained by boiling of NP surrounding. It is also worth noting that the value of the spatial temperature maximum for a nanostructure with Ag NPs has very similar dependence on the surface occupation density and NP radius. Probably, this is due to the fact that two noble metals (Au and Ag) are characterized by close values of the bulk heat capacity.

Note that rise/fall times of the temperature spatial maximum have been measured between 0.1–0.9 levels [44]. Simulation shows that, in general, the transient time slightly increases with increasing of surface occupation density at the constant NP radius for simulated nanostructures. The transient time increases with increasing NP radius at the constant surface occupation density. In particular, rise time increases from 15 to 23 ns for nanostructures with Ag and Au NPs with radius of 15 nm, and it increases from 52 to 128 ns for nanostructures with Ag and Au NPs with radius of 40 nm – both with increasing of the surface occupation density in the range of 10 – 70%. It should be noted that rise and fall times of the temperature for simulated nanostructures are quite close in the studied ranges of microscopic parameters. This is due to equilibrium heating/cooling in the "substrate – NP – neighboring NPs – surrounding" system [14, 21, 45].

Transient times, as well as maximum temperatures, have close values for both metals considered. This is due to the fact that both metals have close values of volumetric heat capacity (for example, for large NPs and macroscopic bodies, it is equal to the product of the specific metal heat capacity and density: 2.46 J/(cm^3 K) and 2.49 J/(cm^3 K) at a temperature of 20°C for Au and Ag respectively [49]). However, the position of the temperature spatial maximum is different for the considered metals, but detailed description is beyond the scope of this work. Further, for definiteness, dependences for Ag NPs will be considered.

Figure 5 shows rise and fall time for temperature spatial maximum versus radius and surface occupation density of the spherical Ag NPs at the optical fiber edge within air. One can see that transient times are approximately constant (with a very small tendency to increase) for simulated nanostructures while increasing of surface occupation density at the constant NP radius. This is correct with the exception of the parameter set, where the surface occupation density is less than 20%, but even in this case the deviation from constant is not exceeding 10%. The rise time increases from 25 ns to 275 ns for simulated nanostructures with increasing NP radius at the constant surface occupation density, at that the steepness of this dependence increases for large radii. This is associated with an increase in the volume fraction of metal in the nanostructure. The fall time increases from 25 ns to 300 ns for simulated nanostructures with increasing NP radius at the constant surface occupation density, at that the steepness of this dependence increases for large radii.

Figure 6 shows rise and fall time for temperature spatial maximum versus radius and surface occupation density of the spherical Ag NPs at the optical fiber edge within air. One can see that rise and fall time for temperature spatial maximum values are very close. Transient time increases for simulated nanostructures with increasing of surface occupation density at the constant NP radius. Rise time increases from 10 ns to 170 ns for simulated nanostructures with increasing NP radius at the constant surface occupation density. This also takes place with an increase in the volume fraction of NPs in the nanostructure. Other conditions being equal, the operation frequency range for nanostructures (operation frequency range is inversely proportional to transient time [14]) in air is wider than for the case of water. This fact is explained by a much larger volumetric heat capacity of water than air (4.18 J/(cm^3·K) for water and $1.30 \cdot 10^{-3}$ J/(cm^3·K) for air).

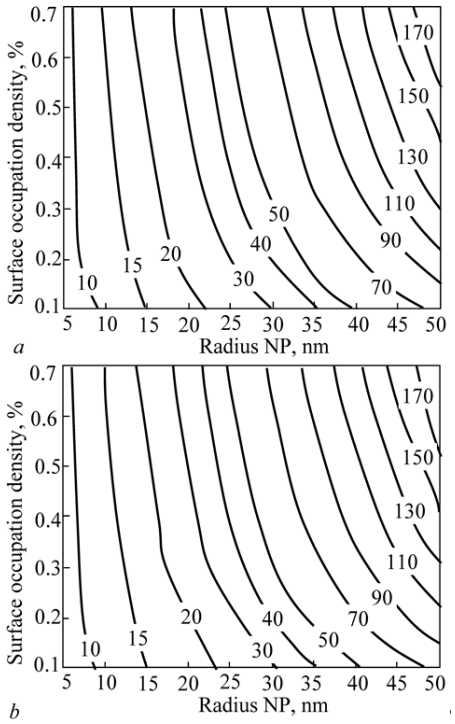

Fig.6. Rise (*a*) and fall (*b*) time for temperature spatial maximum versus radius and surface occupation density of the spherical Ag NPs at the optical fiber edge within air

Figure 7 shows maximal transient time for temperature spatial maximum versus radius and surface occupation density of the spherical Ag NPs at the optical fiber edge within air and water. The maximum transient time for the nanostructure is the longest of the rise and fall times. One can see that the transient time for nanostructures increases with increasing of surface occupation density at the constant NP radius. Operation frequency range for nanostructures in air is wider than for the case of water. In other words, nanostructures are faster in air, since the thermal inertia is much lower. E.g., in addition to the heating of NPs, heating of the surrounding water layer with a high volumetric heat capacity also occurs. The color-filled figures show the regions of effective absorbtion of modulated optical signal. One can see that duration of transients is 10–20 ns for nanostructures with Ag NPs in air; and that duration of transients is 15–50 ns for nanostructures with Au NPs in air. Duration of transients is less than 25 ns for small NPs with a size of ~10 nm, and in the range of 50 – 180 ns for NPs with radii of 15 - 35 nm in water (corresponds to operation frequencies exceeding 10 MHz). For Au nanostructures in water, duration of transients is 35 – 300 ns. Note, there is set of Au nanostructure parameters in water with radii of 22–32 nm and a surface occupation density of 10–22%, but the possibility of such nanostructures usage is limited by overheating.

Thus, the type of nanostructure for photoacoustic transducer, should be selected based on a compromise between the performance requirements (Ag nanostructures

are faster or, in the other words, have wider operation frequency range), and realization simplicity (technological tolerances for Ag nanostructures are more stringent). It should also be noted that overheating is possible for Ag nanostructures in water for heat emission power of 50 mW.

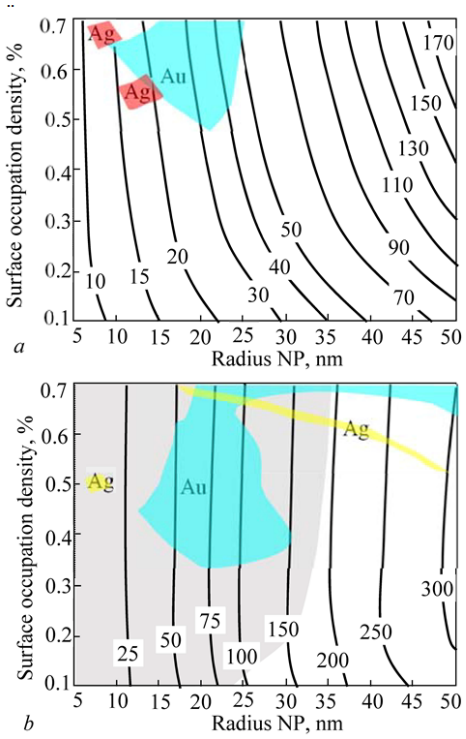

Fig.7. Maximal transient (between levels 0.1 – 0.9) time for temperature spatial maximum versus radius and surface occupation density of the spherical Ag NPs at the optical fiber edge within air (*a*) and water (*b*)

Thermal expansion and acoustic characteristics

To evaluate the efficiency of photoacoustic conversion, it is necessary to calculate the acoustic energy released during the heat release period in the nanostructure [14]:

$$E_{ac} = \frac{\upsilon}{K} S \int_0^T p_{eff}^2(t)\,dt \tag{1}$$

where: υ – the sound speed in surrounding (water or air); K – the bulk modulus of elasticity; S – is the spot area, which is equal to the area of the unit cell simulated, T – the period of the laser pulses, p_{eff} – the effective value of the pressure in the structure cross section; t – time.

The numerical calculation of the photoacoustic conversion efficiency is possible in the following form [14]:

$$\eta = E_{ac}\left[\int_0^T S_{21} P_{LD}(t)\,dt\right]^{-1} \tag{2}$$

where: η – the efficiency, S_{21} – the absorbtion coefficient in the nanostructure, P_{LD} – is the laser radiation power in the optical fiber, E_{ac} – acoustic energy released during the heat release period in the nanostructure. The integral in the expression represents the energy of the laser pulse.

Figure 8 shows pressure distribution in the cross section parallel to the optical fiber edge (the distance between planes is three NP radius) at time instances of 0.125τ and 0.500τ, where laser pulses period τ is 1000 ns. For the nanostructure shown, transient time is 60 ns. One can see that hydrostatic pressure up to 6 MPa is reached near the NP surface (at a distance equals to NP). In this case, the maximum pressure is reached directly above the NP, and the front of the maximum pressure moves along the axis of the optical fiber.

For a nanostructure based on Ag NP with radius of 20 nm, a surface occupation density of 60% in water (parameters are from figure 7), the photoacoustic conversion efficiency near the NP surface (at a distance of NP radius from the nearest NP point) is $2.9 \cdot 10^{-1}$. However, this value is only estimation because of scattering of acoustic waves away from the photoacoustic transducer. As a result of simulation, it was found that this value can decrease by 10^1 – 10^3 times at distances up to 2 mm from the photoacoustic transducer. It is necessary to note that in experimental studies, a value of $1.8 \cdot 10^{-3}$ is reported for a hydrophone located at a distance of 1 mm from a multilayer nanostructure with close NP parameters [21]. Thus, the theoretical result obtained is in a good agreement with experimental data.

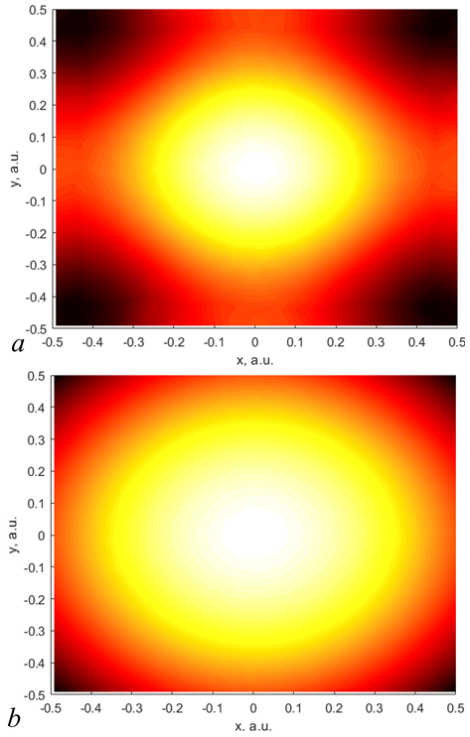

Fig.8. Pressure distribution in the cross section parallel to the optical fiber edge (the distance between planes is three NP radius) at time instances of 0.125τ (*a*) and 0.500τ (*b*), where laser pulses period τ is 1000 ns; the most light color corresponds to maximum pressure of 6 MPa; color scale is linear, Ag NP radius is 20 nm, surface occupation density is 65%; surrounding is water; on the figure, the full unit cell simulated is shown

With regard to the real uses of photoacoustic transducers, photoacoustic conversion efficiency of even 10^{-6} is sufficient for conventional optical absorbers [14]. Thus, fiber-optic photoacoustic transducers based on surface nanostructures allows, at least, increasing the efficiency of photoacoustic conversion by several orders of magnitude compared to traditional optical absorbers in the case of careful study of the relationship between nanostructure microscopic and macroscopic parameters.

Experimental verification

Silver NPs monolayer has been deposited on the optical fiber edge using pulsed laser deposition method. The pulsed YAG:Nd^{3+} pulse-laser LOTIS-TII with a wavelength of 1064 nm and beam intensity of $1.8 \cdot 10^9$ W/cm^2 within the diameter of 1 mm has been used for experiments. Laser

pulse has been focused on a silver 99.99% target (it was constantly moved to provide initial surface for ablation), which is mounted at angle of 45° with respect to the laser beam propagation. Preparation of the surface nanostructure for prototype of photoacoustic transducer has been carried out at room temperature with the typical exposure time for of 2–3 min (~600–900 laser 20 ns pulses).

Figure 9 shows the microphoto of photoacoustic transducer surface with monolayer of silver nanoparticles before measurement of acoustic signal (obtained with scanning electron microscope Hitachi S-4800). One can see that shape of NPs is spherical. The analysis of binarized photos of series allows to conclude that NPs are characterized by gamma-distribution with average size of 35 nm, RMS size variation of 12 nm and surface occupation density of 3.8%.

Figure 10 shows photo of the setup for investigation of a fiber-optic photoacoustic transducer with nanoparticles monolayer deposited on the optical fiber edge within liquid surrounding. TiePie HS5 (oscilloscope coupled with arbitrary waveform generator) generates probe pulses with a period of 10 ms, a duration of 50 ns, fronts less than 12 ns, and an amplitude of 12 V from a digital arbitrary waveform generator. Probe electrical pulses are guided towards to fiber-coupled laser Laserscom LDI-450-FP-30 by means of coaxial cable. The optical signal parameters within the optical fiber are measured by means of 1%:99% fiber-optic coupler, Vishay BPF34 photodiode and control channel of TiePie HS5. The peak optical power at 450 nm is estimated as high as 40 mW.

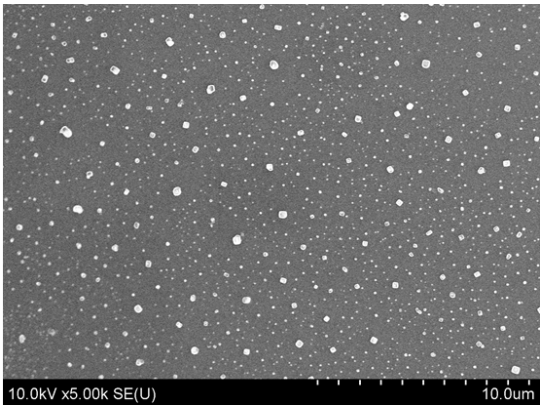

Fig. 9 Microphoto of photoacoustic transducer surface with monolayer of silver nanoparticles before measurement of acoustic signal (obtained with scanning electron microscope Hitachi S-4800)

The most part of the intensity-modulated optical signal (99%) is connected via a Seikoh Giken SNA-1 fiber-optic adaptor the SMF-28e optical fiber with deposited surface nanostructure. The prototype of photoacoustic transducer, in turn, is positioned by Standa 7T38 XYZ system. An acoustic signal is detected by a SoarPiezo 10x0.20mm-PZT5 narrowband hydrophone.

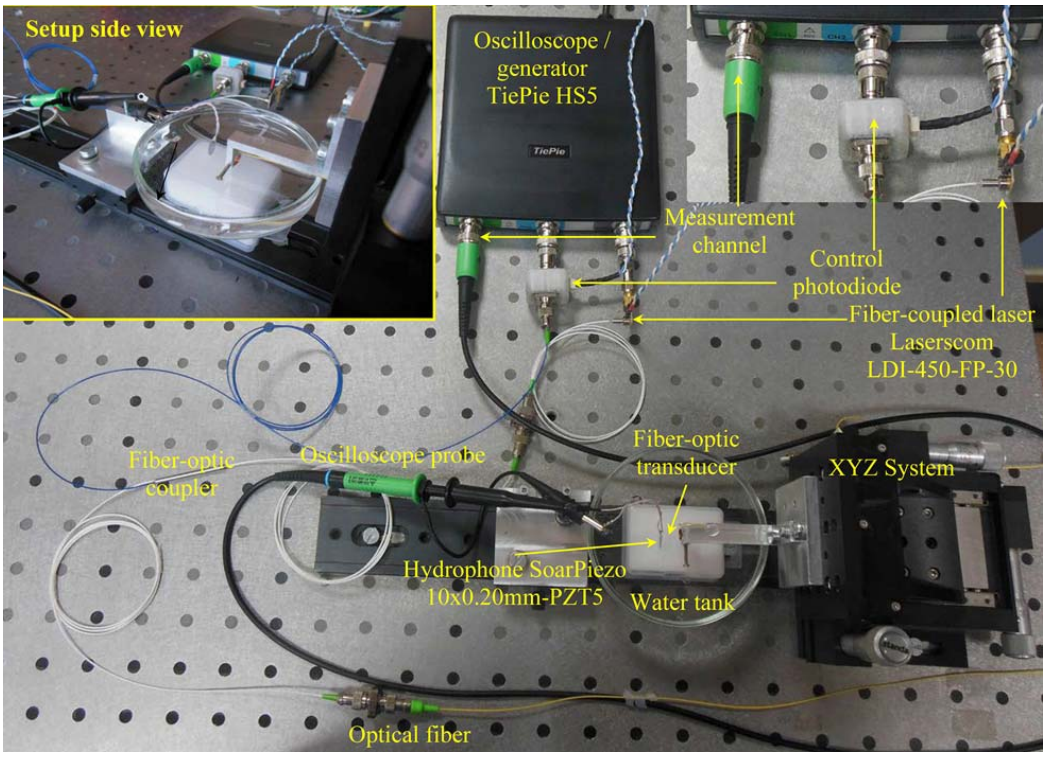

Fig. 10. Photo of the setup for investigation of a photoacoustic transducer with nanoparticles monolayer deposited on the optical fiber edge within liquid surrounding

The hydrophone signal is detected by the measurement channel of high dynamic range oscilloscope TiePie HS5 (a maximal relative uncertainty of signal level measurement is 0.25%). The operation frequency range of the proposed setup exceeds 40 MHz. Figure 11 shows measured power spectrum density of the output signal for the prototype of photoacoustic transducer with monolayer of silver nanoparticles within water surrounding. The power spectral density of the electrical signal at the hydrophone output [V^2/Hz] is directly proportional to the energy [J] and is determined by the acoustic energy [Pa^2]. One can see that the photoacoustic response is observed in the frequency range of 10-18 MHz and its level is more than 12 dB higher

than setup noise floor. This result is in a good agreement with simulation results in figure 7.

Figure 12 shows the microphoto of photoacoustic transducer surface with monolayer of silver nanoparticles after the 1 hour measurement of acoustic signal. One can that there is no observable effect of 1 hour operation on the surface nanostructure microscopic parameters. This fact makes it possible to use such transducers as part of high-resolution technical diagnostic and non-destructive testing systems.

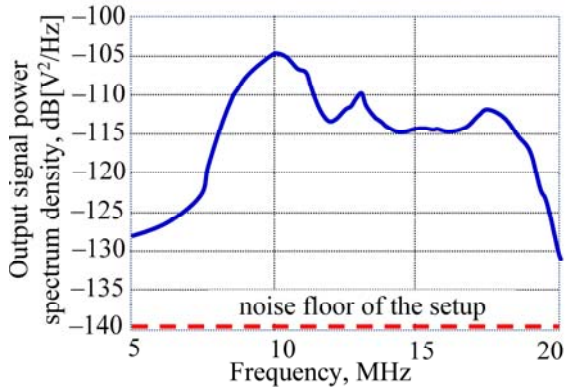

Fig.11. Power spectrum density of the output signal for the prototype of photoacoustic transducer with monolayer of silver nanoparticles within water surrounding

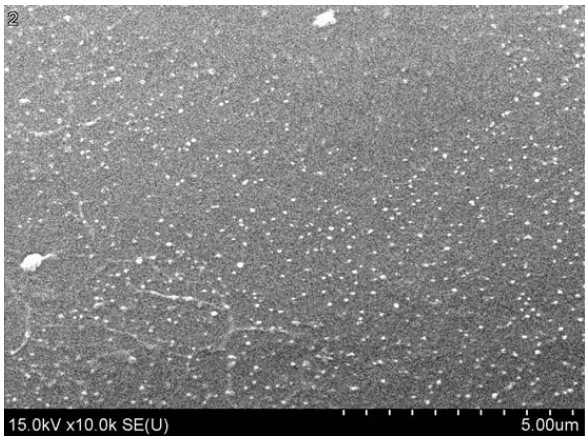

Fig. 12 Microphoto of photoacoustic transducer surface with monolayer of silver nanoparticles after measurement of acoustic signal (obtained with scanning electron microscope Hitachi S-4800)

Conclusion

Comprehensive simulation of optical, thermophysical and acoustic properties of surface nanostructures with metallic nanoparticles for fiber-optic photoacoustic ultrasound transducers is presented. This approach allows to establish relationship between nanostructure microscopic parameters, modulated optical power and the output acoustic characteristics of the photoacoustic transducer.

It is shown that the applicability of surface nanostructures in air as photoacoustic transducer is not limited by thermal destruction of the nanostructure, while the thermophysical limitations for nanostructures in water are explained by boiling. It is shown that, other conditions being equal, the operation frequency range for nanostructures (operation frequency range is inversely proportional to transient time) in air is wider than for the case of water.

Comprehensive study of nanostructures made it possible to establish that the type of nanostructure for photoacoustic transducer should be selected based on a compromise between the performance requirements (Ag nanostructures are faster), and realization simplicity (technological tolerances for Ag nanostructures are more stringent). For studied nanostructures, the operation frequency range is inversely proportional to transient time, which, in turn, can be as low as 10 – 20 ns.

Design of fiber-optic photoacoustic ultrasound transducer providing the most effective optical-to-acoustic conversion (intensity modulated optical signal is converted into pressure waves) is proposed as a result comprehensive theoretical study of absorbed optical power, stationary and non-stationary temperature and pressure distribution. The photoacoustic conversion efficiency near the NP surface is estimated to $2.9 \cdot 10^{-1}$, but this value can decrease by 10^1 – 10^3 times at distances up to 2 mm from the photoacoustic transducer because of scattering of acoustic waves. The hydrostatic pressure up to some MPa can be achieved near the surface of the NP. The use of fiber-optic photoacoustic transducers based on surface nanostructures allows one to at least increase the efficiency of photoacoustic conversion by several orders of magnitude compared to traditional optical absorbers with the correct selection of microscopic parameters.

In the paper, the photoacoustic response is experimentally observed in the frequency range of 10-18 MHz for surface nanostructure with average size of nanoparticles of 35 nm, RMS size variation of 12 nm and surface occupation density of 3.8%. This is in a good agreement with theoretical results.

The work is supported by grant "BRFFR-RFBR M-2019" No. F19RM-006 “Study of 2D plasmonic nanostructures for photoacoustic transducers”. This work is also a part of a Alena Mikitchuk doctoral thesis.

***Authors**: inż. Alena Mikitchuk and prof. dr hab. inż. Konstantin Kozadaev, Belarusian State University, 4 Nezavisimosti ave., 220004 Minsk, Belarus, E-mail: m.helenay@yandex.by.*

REFERENCES

[1] Hanselka H., Nuffer J. Characterization of reliability. Springer handbook of metrology and testing, Springer (2011), 16.7.
[2] Czichos H. Metrology and testing in materials science and technology, Meas. Sci., 4 (2009), No.4, 48 –77.
[3] Vesely W. [et al.] Fault tree handbook with aerospace applications, NASA (2002), 218.
[4] Mufti A. Guidelines for structural health monitoring, Canada Res. Netw. Man., No.1 (2001).
[5] Worden K. [et al.] The fundamental axioms of structural health monitoring, Philos. T. R. Soc. A., 463 (2007),No.2082, 1639 – 1664.
[6] Czichos H. Handbook of technical diagnostics, Springer (2013), 566
[7] Sposito G. [et. al] A review of non-destructive techniques for the detection of creep damage in power plant steels, NDT Int., 43 (2010), No.7, 555–567.
[8] Snook K.A. [et. al] High-frequency ultrasound annular-array imaging. Part I: array design and fabrication, IEEE Trans. Ultrason. Ferroelectr. Freq. Control, 53 (2006), No.2, 300–308.
[9] Sharples S.D., Clark M., Somekh M.G. Spatially resolved acoustic spectroscopy for fast noncontact imaging of material microstructure, Opt. Expr., 14 (2006), No. 22, 10435–10440.
[10] Baerwald A. [et. al] Use of ultrasound biomicroscopy to image human ovaries in vitro, Ultras. Obstet. Gynecol., 34 (2009), No. 2, 201–207.
[11] Foster F.S. [et. al] A new 15-50 MHz arraybased micro-ultrasound scanner for preclinical imaging Ultras. Med. Biol., 35 (2009), No.10, 1700–1708.
[12] Jadidian B. [et. al] 25 MHz ultrasound transducers with lead-free piezoceramic, 1-3 PZT fiber-epoxy composite, and PVDF polymer active elements, IEEE Trans. Ultrason. Ferroelectr. Freq. Control, V.56 (2012), No.2, 368–378.
[13] Gottlieb E.J. [et. al] Development of a high-frequency (> 50 MHz) copolymer annular-array, ultrasound transducer, IEEE

Trans. Ultrason. Ferroelectr. Freq. Control, 53 (2006), No.5, 1037–1045.
[14] Biagi E., Margheri F., Menichelli D. Efficient laser-ultrasound generation by using heavily absorbing films as targets, IEEE Trans. on ultrason., ferroel. and freq. control, 48 (2001), No. 6, 1669 – 1679.
[15] Buma T., Spisar M., O'Donnell M. A high-frequency, 2-D array element using thermoelastic expansion in PDMS Trans. Ultrason. Ferroelectr. Freq. Control, 50 (2003), No.9, 1161–1176.
[16] Hou Y. [et. al.] Characterization of a broadband all-optical ultrasound transducer—from optical and acoustical properties to imaging, Appl. Phys. Lett., 91 (2007), Art. No.073507.
[17] Wu Nan. [et al.] Fiber optic ultrasound transmitters and their applications, Measurement, 79 (2016), 164 – 171.
[18] Won Baac, H. Carbon nanotube composite optoacoustic transmitters for strong and high frequency ultrasound generation, Appl. Phys. Lett., 97 (2010), No.23, Art. No. 234104.
[19] Hu Chennan, Yu, Zhihao, Wang, Anbo An all fiber-optic multi-parameter structure health monitoring system, Opt. Express, 24 (2016), No.18, 20287 – 20296.
[20] Tian Y. Fiber-optic ultrasound generator using periodic gold nanopores fabricated by a focused ion beam, Opt. Eng., 52 (2013), No. 6, Art. No. 065005.
[21] Zou X. [et. al] Broadband miniature fiber optic ultrasound generator, Opt. express, 22 (2014), No. 15, 18119 – 18127.
[22] Hou Y. [et. al] Characterization of a broadband all-optical ultrasound transducer-from optical and acoustical properties to imaging, IEEE Trans. Ultrason. Ferroelectr. Freq. Control, (2008) 55, No. 8, 1867–1877.
[23] Smith R. [et al.] Design and fabrication of nanoscale ultrasound transducers, J. Phys. Conf. Ser., 278 (2011), Art. No. 012035.
[24] Zou X. [et. al] Polydimethylsiloxane thin film characterization using all-optical photoacoustic mech., Appl. Opt., 52 (2013), No.25, 6239–6244.
[25] Hou Y. [et. al] Broadband all-optical ultrasound transducers, Appl. Phys. Lett., 91 (2007), No.7, Art. No. 073507.
[26] Zhou Jingcheng High temperature monitoring using a novel fiber optic ul-trasonic sensing system, Proc. of Micro- and Nanotechnol. Sens., Syst., and App.,10639 (2018), Art. No. 1063910.
[27] Wu N. [et. al] High-efficiency optical ultrasound generation using one-pot synthesized polydimethylsiloxane-gold nanoparticle nanocomposite, J. Opt. Soc. Am. B, 29 (2012), No.8, 2016–2020.
[28] Ortega-Mendoza J.G. [et al.] Selective photodeposition of zinc nanoparticles on the core of a single-mode optical fiber, Opt. Express, 21 (2013), No.5, Art. No. 6509.
[29] Hunter A.J., Drinkwater B.W., Wilcox P.D. Autofocusing ultrasound imagery for non-destructive testing and evaluation of specimens with complicated geometries, NDT Int., 43 (2010), No.2, 78–85.
[30] Rivero P.J. [et al.] Localized surface plasmon resonance for optical fiber-sensing applications, Nanoplasmonics – Fundamentals and applications, Intech (2017), 399 – 429.
[31] Mikitchuk A.P., Kozadaev K.V. Simulation of the optical properties of surface nanostructures for photoacoustic transducers, Quant. El., 48 (2018), No. 7, 630 – 638.
[32] Mikitchuk A.P., Kozadaev K.V. Photoacoustic generation with surface noble metal nanostructures, Proc. of Int. Symp. "Nanostruct.: Phys. and Technol.", Minsk (2018), 97 – 98.
[33] Kozadaev K.V. Diagnostics of aqueous colloids of noble metals by extinction modeling based on Mie theory, J. of Appl. Spectroscop., 78 (2011), No. 5, 692–697.
[34] Goncharov V.K., Kozadaev K.V., Shchegrikovich D.V. Investigation of noble metals colloidal systems formed by laser synthesis at air, Adv. in Opt. Tech., 1 (2012), Art. No. 907292.
[35] Mikitchuk A.P. Kozadaev K.V., Photoacoustic generation with surface noble metal nanostructures, Semiconductors., 52 (2018), No. 14. 1839 – 1842.
[36] Mikitchuk A.P., Kozadaev K.V. Convergence for simulation of surface nanostructure optical properties using finite integral technique, Phys. and chem. asp. of the study of clust., nanostruct. and nanomater., 10 (2018), 460 – 467.
[37] Mikitchuk A.P., Kozadaev K.V., Simulation of the electromagnetic properties of silver nanostructures on the solid substrate in the air atmosphere, J. of the Bel. St. Univ.. Phys., 1 (2017), No. 1, 100 – 107.
[38] Nishijima Y., Rosa L., Juodkazis S. Surface plasmon resonances in periodic and random patterns of gold nano-disks for broadband light harvesting, Opt. Express, 20 (2012), No. 10, 11466 – 11477.
[39] Pozar D.M. Microwave Engineering, John Wiley & Sons (2012), 228.
[40] Fritzen F., Bohlke T. Influence of the type of boundary conditions on the numerical properties of unit cell problems, Tech. Mech., 30 (2010), No. 4, 354–363.
[41] Goncharov V.K., Kozadaev K.V., Mikitchuk A.P., Diagnostics of the monolayer silver nanostructures on a solid substrate using the bifactorial analysis of the SPR band, High temp. mat. process., 18 (2014), No. 3, 201–213.
[42] Kreibig U., Vollmer, M. Optical properties of metal clusters, Springer-Verlag (1995), 436.
[43] Hutter T., Elliott S.R., Mahajan S., Interaction of metallic nanoparticles with dielectric substrates: effect of optical constants, Nanotechnol., 24 (2013), 035201 – 035209.
[44] Matasane C.M., Kahn M.T.E. Measurement of thermal and transient responses in optical fiber, EngineerIT (2008), 31 – 32.
[45] Horikoshi S., Kato T., Theoretical study of the interparticle interaction of nanoparticles randomly dispersed on a substrate, J. of Appl. Phys., 117 (2015), Art. No. 023117.
[46] Mikitchuk A.P., Kozadaev K.V., Modelling the interaction between silver nanoparticles in a monolayer on a glass substrate, J. of Appl. Spectroscop., 83 (2017), No.6, 947–952.